Journal of the Meteorological Society of Japan, Vol. 76, No. 4, pp. 663–671, 1998

NOTES AND CORRESPONDENCE

Satellite-Derived Vegetation Index and Evapotranspiration Estimated by Using Assimilated Atmospheric Data over Asia

By Rikie Suzuki[1]

Frontier Research System for Global Change, c/o National Research Institute for Earth Science and Disaster Prevention, Tsukuba 305-0006, Japan

Akiyo Yatagai

National Space Development Agency of Japan, Earth Observation Research Center, Tokyo 106-0032, Japan

and

Tetsuzo Yasunari

Institute of Geoscience, University of Tsukuba, Tsukuba 305-8571, Japan

(Manuscript received 22 November 1996, in revised form 22 May 1998)

Abstract

The monthly evapotranspiration (ET), which was estimated from assimilated atmospheric data from European Centre from Medium-Range Weather Forecasts (ECMWF) and gridded global precipitation data introduced by Xie and Arkin, was examined in relation to the vegetation activity for 1987 and 1988 over Asia. The vegetation activity was represented by the Normalized Difference Vegetation Index (NDVI) that was calculated from satellite observation.

Over Siberia, the annual marches of the ET and the NDVI were quite similar. Furthermore, bimodal annual variations of the NDVI and ET were observed in Punjab (around Pakistan and northern India) where bi-seasonal cultivation is seen. The ET–NDVI relationships were analyzed for seven vegetational cover types and revealed that slopes of ET–NDVI regression lines are distinguished depending on the vegetation types. The results presented in this paper demonstrate the possibility of investigating the continental-scale vegetation activity and the ET, which is derived from assimilated gridded global data.

1. Introduction

The main energy sources for the atmospheric circulation are the sensible and latent heats provided from Earth's surface. The investigation on surface processes, such as water and energy exchanges which take place at Earth's surface, gives us a better understanding of the global climate system. Among the surface processes, the role of the vegetation activity should be considered, because the evapotranspiration (ET) is strongly controlled by vegetation cover with its transpiration activity and canopy structure (*e.g.*, Ripley and Redmann, 1976). This study will focus on the relationship between the vegetation activity and the ET over Asia.

From the 1980s, global vegetation data have been provided by satellite observation from space. The difference of spectral reflectance of chlorophyll pigment between the visible and near-infrared parts of the spectrum provides the means for monitoring density and vigor of green vegetation (*e.g.*, Tarpley *et al.*, 1984). The NOAA satellite has a five-

1 Corresponding author: Rikie Suzuki, Frontier Research System for Global Change, c/o National Research Institute for Earth Science and Disaster Prevention, Tsukuba 305-0006, Japan. E-mail: suzuki@frontier.bosai.go.jp

channel on-board radiometer, called the Advanced Very High Resolution Radiometer (AVHRR). Channels 1 (red: 0.58–0.68 μm) and 2 (near-infrared: 0.73–1.10 μm) correspond to the visible and near-infrared spectral bands. The Normalized Difference Vegetation Index (NDVI), which is the most well-known vegetation index, is computed from following equation (*e.g.*, Tarpley *et al.*, 1984):

$$NDVI = \frac{Ch2 - Ch1}{Ch2 + Ch1} \tag{1}$$

where $Ch1$ and $Ch2$ are values from AVHRR Channels 1 and 2, respectively. The NDVI ranges from -1.0 to 1.0. For the actual Earth surface, NDVI ranges from -0.1 to 0.6. This remotely sensed value of the NDVI allowed us to analyze global vegetation conditions. For example, global vegetation cover classifications have been performed according to the NDVI-derived phenological characteristics of vegetation (*e.g.*, Norwine and Greegor, 1983; DeFries and Townshend, 1994).

Many previous studies analyzed the relationships between the ET, which is the subject of this study, and the NDVI-derived vegetation activity (*e.g.* Running and Nemani, 1988; Running *et al.*, 1989). However, the areas analyzed by these studies were relatively small, for example, Running and Nemani (1988) analyzed the NDVI in a 15 × 15 km pixel at seven meteorological stations. A couple of studies, which targeted the large-scale ET and the NDVI, were published. Kondoh (1995) analyzed the relationship between the NDVI and ET, which was estimated from climatological estimation methods, such as, the Brutsaert and Stricker method (Brutsaert and Stricker, 1979) and the Morton method (Morton, 1979), *etc.*, over south Asia. Matsuyama *et al.* (1994) studied the hydrological cycle, including the ET, in the Congo basin in relation to the NDVI.

In this study, we focus on the continental-scale relationship between the NDVI and the ET over Asia. The ET is estimated from the gridded monthly precipitation data and the moisture divergence value in the atmosphere using European Centre for Medium-Range Weather Forecasts (ECMWF) four-dimensionally assimilated atmospheric data. The availability and feasibility of such assimilated data have been discussed in many articles in recent years (*e.g.*, Trenberth and Olson, 1988; Trenberth, 1991; Trenberth and Guillemot, 1995). This method has the advantage that no parameterization is required for surface conditions, which are usually very complex and difficult to evaluate.

2. Data and analyses

We surveyed the NDVI and ET for 1987 and 1988 over the region bounded by 40°E, 160°E, 4.5°N, and 75°N, which covers Asian regions. These two years have been intensively investigated by international researchers, working on projects such as the International Satellite Land Surface Climatology Project (ISLSCP) (Sellers *et al.*, 1996). All the analyses are performed on a monthly basis, which corresponds to the temporal resolution of the precipitation data.

2.1 Global Vegetation Index

The monthly NDVI is obtained from the Global Vegetation Index (GVI) data set (*e.g.*, Tarpley, 1991), that has 0.144° × 0.144° resolution. The monthly NDVI value was represented by the maximum NDVI of four (or five) weekly GVI for each pixel in each month (*e.g.*, Murai and Honda, 1991; Honda *et al.*, 1992). This process should be more efficient in removing the cloud cover from the monthly GVI than averaging weekly GVIs.

2.2 Evapotranspiration

The ET from the surface can be estimated from the water budget in the atmosphere, which was discussed in Peixoto and Oort (1983, 1992). The evapotranspiration E from the bottom (*i.e.*, ground surface) of an air column, which vertically extends from the ground surface to the top of the atmosphere, can be expressed by the following atmospheric water budget equation,

$$E = P + \frac{\partial W}{\partial t} + \nabla_H \cdot \vec{Q} \tag{2}$$

where t is the time; P, the precipitation at the bottom; W, the precipitable water in the air column; and $\nabla_H \cdot \vec{Q}$, the horizontal flux divergence of water vapor integrated from the surface to the top of atmosphere (so called "aerial runoff"). In the actual atmosphere, there is water transportation by condensed water, such as cloud water. However, the amount and flux of condensed water is usually much less than that of water vapor in the atmosphere (*e.g.*, Peixoto and Oort, 1992). In this regard, its component is not included in Eq. (2).

This study assumed 2.5°×2.5° (longitude and latitude) air columns over the region, and computed ET for each grid cell. For the monthly precipitation P, the "the merged analysis of precipitation of Xie and Arkin (version 9607)" dataset (Xie and Arkin, 1995, 1996) was used. This global precipitation product (2.5° × 2.5° spatial resolution) was a composite of several kinds of data sources such as gauge observation, satellite estimates of infrared and microwave, and numerical model outputs. Gauge measurements are used to estimate precipitation over the land.

It is possible to compute the terms $\partial W/\partial t$ and $\nabla_H \cdot \vec{Q}$ from the specific humidity and wind data. In the present study, gridded data provided by ECMWF are used to calculate $\partial W/\partial t$ and $\nabla_H \cdot \vec{Q}$. The initial values for their forecasting (known as ECMWF/WMO analysis) are utilized.

Twice daily (0000 and 1200 GMT) aerological values of the ECMWF's data on each 2.5° × 2.5° grid point were produced by a dynamically consistent temporal extrapolation using the General Circulation Model (GCM), and the statistical spatial interpolation of the observed data (rawinsondes, satellite temperature and moisture, *etc.*) was performed using the optimum interpolation method. Wind, humidity, and geopotential height values at seven standard pressure levels (1000, 850, 700, 500, 300, 200, 100 hPa) are available.

The monthly $\nabla_H \cdot \vec{Q}$ for each 2.5° × 2.5° grid cell in 1987 and 1988 was estimated by integrating the flux divergence from the ground to 100 hPa (Oki *et al.*, 1995; to be referred as Oki-95). The monthly $\partial W/\partial t$ was calculated from precipitable water difference between the beginning and end of each month. Topography, the ground surface height information, on a 2.5° × 2.5° grid was obtained from ETOPO5 (EPA Global Climate Research Program and NOAA/NGDC Global Change Database Program, 1992), a digital elevation map of five minutes spatial resolution.

Before April 7, 1987, there was no vegetational factor in the land-surface parameterization of the ECMWF's GCM. After April 7, 1987, the vegetational factor was parameterized according to the fractional area of vegetation to each grid cell. According to Blondin (1991), the factors of soil moisture and radiation stress factor are considered in the calculation of the canopy resistance, while the parameter for vegetation seasonality was held constant (*i.e.*, no seasonal change).

The estimation precision of the ECMWF 4DDA dataset may still be improved (*e.g.*, Trenberth and Guillemot, 1995), however it is one of the most applicable objective analysis datasets for global climatological studies. In recent years, more accurate assimilated data has become available as "re-analysis data" (*e.g.*, Kalnay *et al.*, 1996). However, recent data are often parameterized by the seasonal change of the vegetation. In this respect, we used the old version of ECMWF assimilated dataset that is not parameterized for the seasonal cycle of vegetation.

A discussion on the estimation accuracy of $\nabla_H \cdot \vec{Q}$ in Eq. (2) can be found in Oki-95, that estimated monthly $\nabla_H \cdot \vec{Q}$ on the globe. Oki-95 used the same version of ECMWF data as this study. The scheme for estimating $\nabla_H \cdot \vec{Q}$ is also substantially the same as in this study. In this regard, the discussion on the accuracy of the estimation made by Oki-95 is applicable to this study.

If the water storage in a basin is not changeable, the annual discharge from the basin is equal to the annual $P - E$ in the atmosphere above the basin. Applying this principle, Oki-95 compared a four-year mean estimated $-\nabla_H \cdot \vec{Q}$ with the climatological mean of observed runoff in 70 river basins, and concluded that they showed good agreement, especially in mid and high latitudes of the northern hemisphere. In addition, Oki-95 revealed that the seasonal change of the estimated ET corresponded very well with the river runoff by investigating the water balance in Chao Phraya river basin. For this reason, it will be reasonable to discuss $\nabla_H \cdot \vec{Q}$ and its seasonal change, which is our main concern in this study.

3. Distributions of the estimated ET

Figure 1 presents examples of estimated ET for each 2.5° × 2.5° grid cell in January and July 1987. These ET values in Fig. 1 are horizontally moving-averaged by nine grid cells. The ET over the ocean is generally larger than over land, which suggests a greater potential of the ET from the sea surface than that from the land surface. Over Siberia, the ET is very low in January.

In July, a large ET can be found in the southern part of the region, especially over the Indian Ocean. The active summer monsoon there probably induces a large amount of ET. Over Siberia, an ET of several tens of millimeters per month is found. The wet land cover probably provides water vapor through transpiration and direct evaporation from soil at high temperatures.

The estimated ET exhibits a considerably negative value mainly around western Pakistan, eastern India, and western Tibet in the July map. Those areas, which have a considerably negative ET, seem to be concentrated in regions with complicated topography. This somewhat non-realistic estimation may be mainly caused by the insufficient spatial resolution of the ECMWF and gridded precipitation dataset. Although the accuracy of the absolute value of the ET should be improved in some parts of the region, we consider that the seasonal fluctuation of the estimated ET should represent the actual ET variation.

4. Seasonal change of the NDVI and ET

Kondoh (1995) estimated climatological monthly ET (both potential and actual ET) over southern Asia by some climatological methods, such as the Brutsaert and Stricker method and the Morton method *etc.*, and indicated seasonal variations of ET at Yichang (30.70°N, 111.17°E) in China. To compare the ET estimated in the present study with Kondoh's estimation, the mean ET over 16 grid cells (110–120°E, 30–40°N), which include Yichang, was calculated, and its monthly change is shown in Fig. 2. Those grid cells were selected not to cover the mountainous area.

As can be seen in Fig. 2, the annual maximum values are approximately 185 mm/month (this study) and 170 to 210 mm/month (actual ET estimated

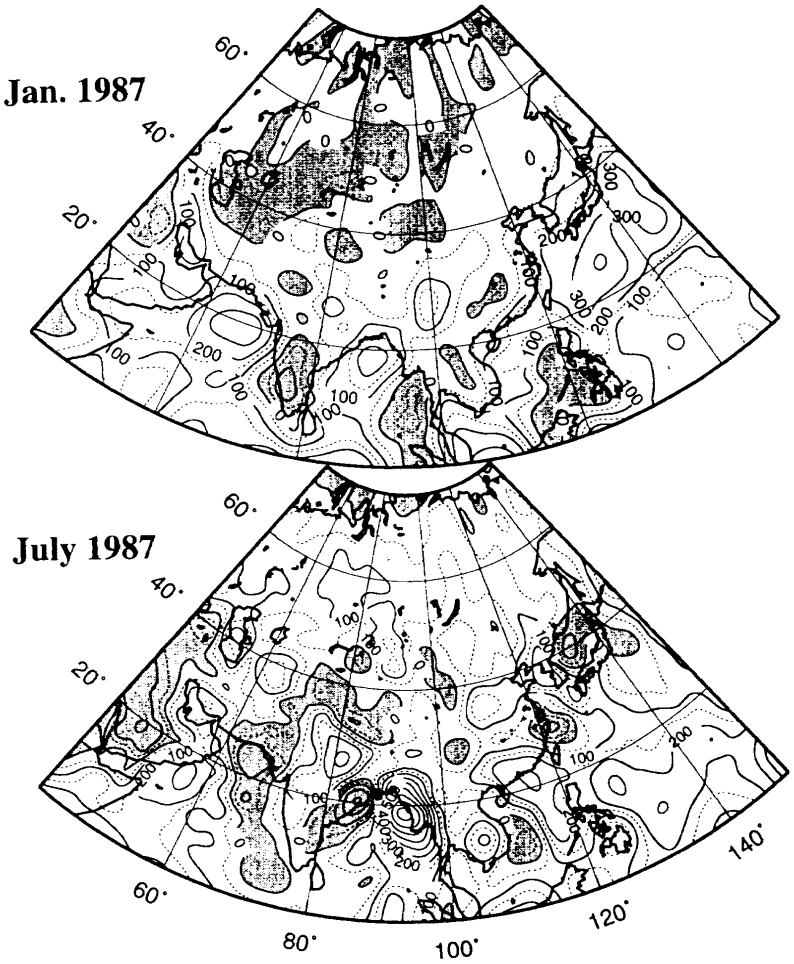

Fig. 1. Examples of the estimated ET (mm/month) distribution over Asian regions, January (upper) and July (lower) in 1987. The distribution is horizontally moving-averaged by nine grid cells. The interval of solid contours is 100 mm/month. Dashed contours are drawn at −50, 50, 150 mm/month.

by Kondoh). Figure 2 also shows that the ET in winter is around 25 mm/month, while Kondoh estimates the actual ET from December to February to be 10 to 30 mm/month. Although the ET shown in Fig. 2 is estimated over 16 grid cells and Kondoh's ET is estimated at a point, the estimates agree well. This fact supports the idea that the ET estimation in this study represents the actual ET.

Figure 3 shows the monthly mean changes of the NDVI and ET over the four rectangular regions that are listed in Table 1 in 1987 and 1988. In western Siberia, a very similar annual fluctuation can be seen between the NDVI and ET. In May, the NDVI plots drastically increase, coincidentally the ET starts to increase. Both subsequently reach the maximum values in July. From October to April, both NDVI and ET have low values. The NDVIs in these months are almost constant (about 0.05).

In eastern Siberia, a similar ET–NDVI seasonal variation is found. However, the maximum values of the NDVI and ET are slightly smaller than those of western Siberia. In addition, the abrupt increase of the NDVI starts in June, one month behind that of western Siberia. These differences may be due to the vegetational differences, such as phenology of the vegetation, but the exact reason is not clear.

In the Punjab area, both NDVI and ET have two apparent peaks by year as indicated in Fig. 3, although the number of grid cells (*i.e.*, 3 cells) may not be enough for the ET estimation. Malingreau (1986) reported that this bimodal seasonal change of NDVI is related to the bi-seasonal cultivation, wheat in spring and rice in summer. The signal of bi-seasonal cultivation may be detected in the estimated ET.

Over the Indo-China peninsula, where tropical rain forest and cultivated land prevail, the relation between the NDVI and ET is less clear than in other regions. In the tropical regions, the cloud contamination on the NDVI is probably considerable, even if we use the monthly maximized NDVI as in the present study. Moreover, the NDVI, which is the satellite-sensed value, cannot seize the vegetation activity in the lower layer in the forest concealed by

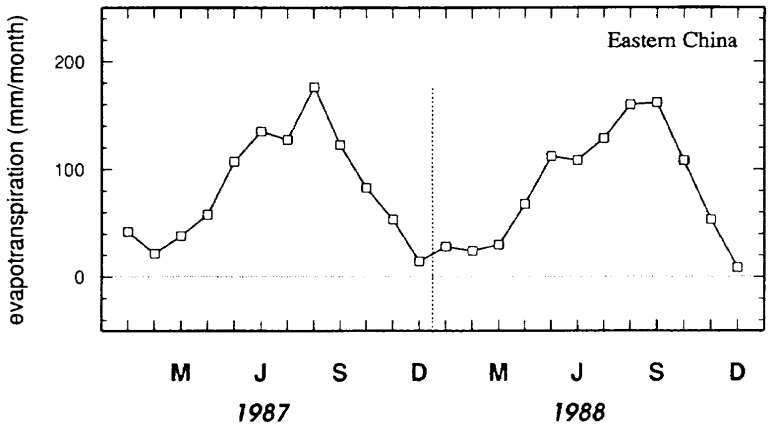

Fig. 2. The seasonal variation of the estimated ET over 16 grid cells in eastern China (110–120°E, 30–40°N).

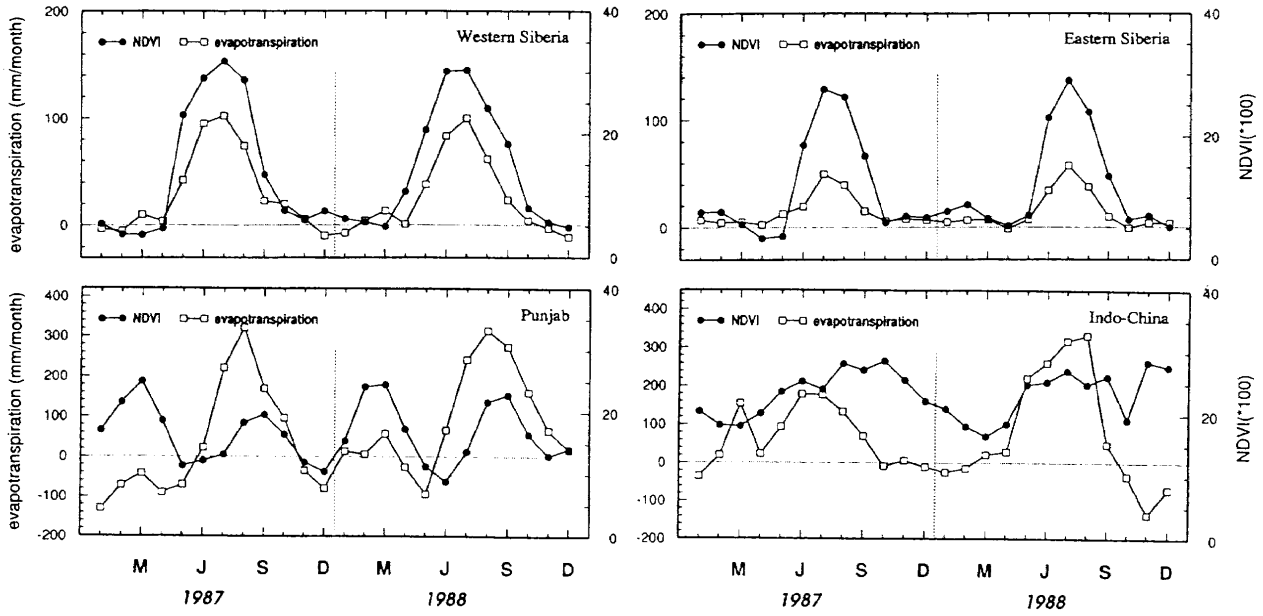

Fig. 3. The seasonal variation of the NDVI and ET over four regions listed in Table 1. Note that the coordinates of the ET are different among the four panels.

the dense canopy of tropical forests. These factors may make the NDVI–ET relation unclear.

These facts reveal that the seasonal variation of the ET coincides with that of the NDVI over some regions but not over tropical regions. It may be that vegetation-induced fluctuations are detected in the ET estimated from the 4DDA system, which is independent of the seasonal vegetation cycle.

The correlation coefficient for each grid cell was calculated using a 24-month time series of the NDVI and ET, and displayed in Fig. 4. Large positive correlation coefficients are found over Siberia and northeast China, suggesting a close relationship between the transpiration activity from the boreal forest and the ET. In contrast, the coefficient is significantly smaller in tropical regions. Some cells in the tropics have negative values. As mentioned, the NDVI–ET relation is unclear due to the effects of cloud contamination and the dense forest. There are some negative correlations around arid regions, which may occur due to a calculation problem, that is, the very small amplitude of the NDVI seasonal change.

5. Vegetation type, NDVI, and ET

The dataset "Olson World Ecosystems" in the CD-ROM "Global Ecosystems Database Ver. 1.0" (EPA Global Climate Research Program and NOAA/NGDC Global Change Database Program, 1992) provides a distribution of 59 vegetation cover types for 10′ × 10′ on Earth. For the present analysis, those 59 types are re-categorized into seven cat-

Table 1. Regions where the ET and NDVI were calculated in Fig. 3. "Number of grid cells" means the number of the ECMWF grid cells that were used for the calculation of mean value of ET in the respective region.

Region	Longitude (°E)	Latitude (°N)	Number of grid cells
Eastern Siberia	100.0—130.0	60.0—70.0	48
Western Siberia	60.0—80.0	50.0—60.0	32
Punjab	70.0—77.5	30.0—32.5	3
Indo-China	100.0—107.5	12.5—17.5	6

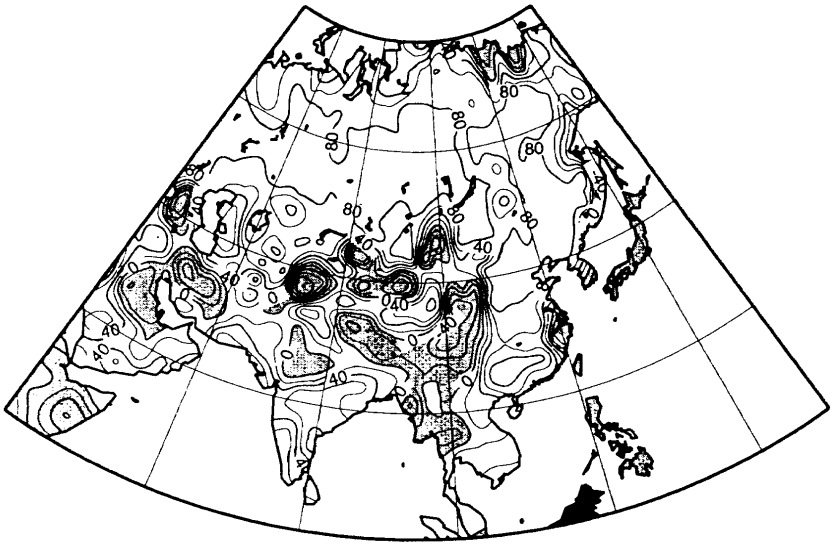

Fig. 4. The distribution of the correlation coefficient (multiplied by 100) between the NDVI and ET seasonal change. The coefficient in grid cells over ocean and coastal areas was not calculated.

egories (from A to G), and the relationship between NDVI and ET is analyzed (see Appendix for the categorization).

Figure 5 displays the geographical distribution of the seven re-categorized vegetation cover types, and Fig. 6, the scatter diagrams of the ET–NDVI relationships for each vegetation category. The monthly mean ET and NDVI values of each vegetation type are plotted in the scatter diagram for 24 months (1987 and 1988).

All regression lines in the scatter diagram exhibit a positive ET–NDVI correlation. This means the ET increases as the vegetation activity strengthens. Moreover, slopes of regression lines can be clearly distinguished depending on the vegetation categories. Over the boreal forest, which mainly spreads over Siberia, the cool climate might not be a suitable condition for active transpiration, although a remarkable seasonal change of NDVI is found. For this reason, the ET–NDVI regression line of B (boreal forest/taiga) may have a steep slope. In contrast, over the warm cultivated land, the ET may change significantly with the season due to the warm climatological condition. In this regard, the regression line of D (warm forest/cropland) has a relatively small slope. Over arid regions such as types F (semi-arid) and G (desert), the seasonal amplitude of the NDVI is very small, while the ET changes significantly. The evaporation from the ground surface may be the predominant factor in the total ET over arid regions where the vegetation activity is low. The scatter diagram for E (tropical forest) exhibits a characteristic regression line, showing almost no correlation due to the small seasonal variation of the NDVI in tropical vegetation.

Of course, the estimated ET involves the evaporation component from the ground surface, and the evaporation also varies with the climatological zones. We did not take into account the meridional systematic trend of NDVI due to the satellite observing geometry. However, the relationships indicated in Fig. 6 may be demonstrating a fundamental characteristic of the relationship between the ET and the vegetation type.

6. Conclusion

The monthly ET, which was estimated from vapor flux divergence and gridded global precipitation data, was examined in relation to the satellite data of the NDVI for 1987 and 1988, and close relation-

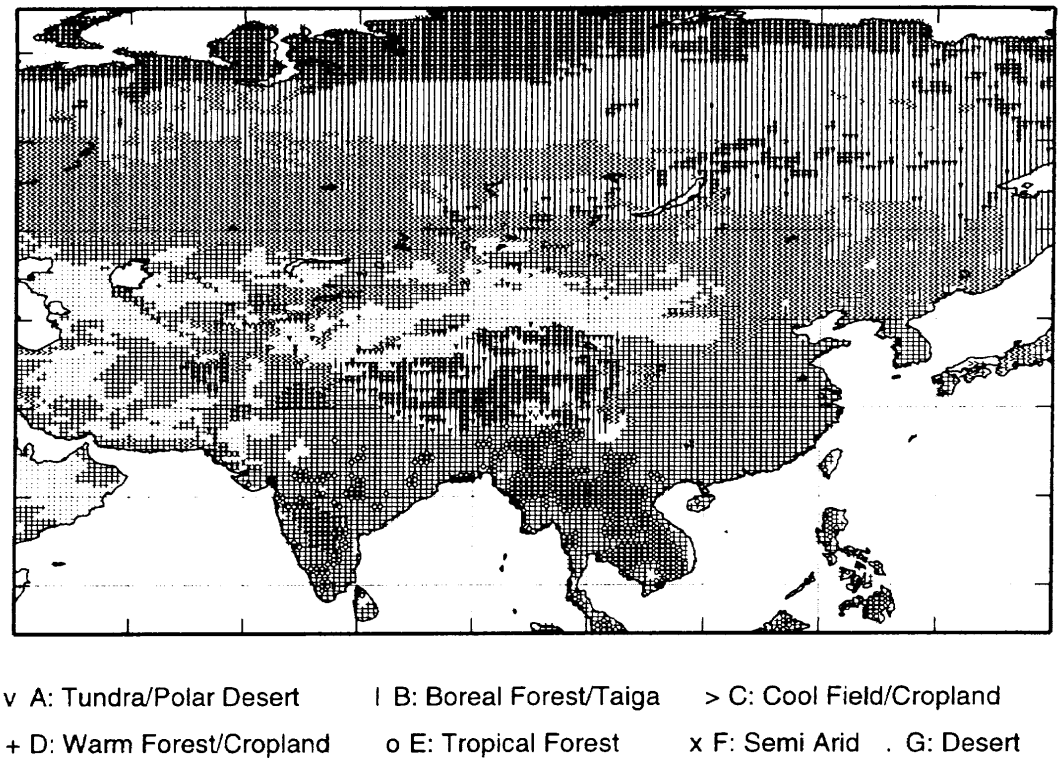

Fig. 5. The distribution of seven vegetation cover types.

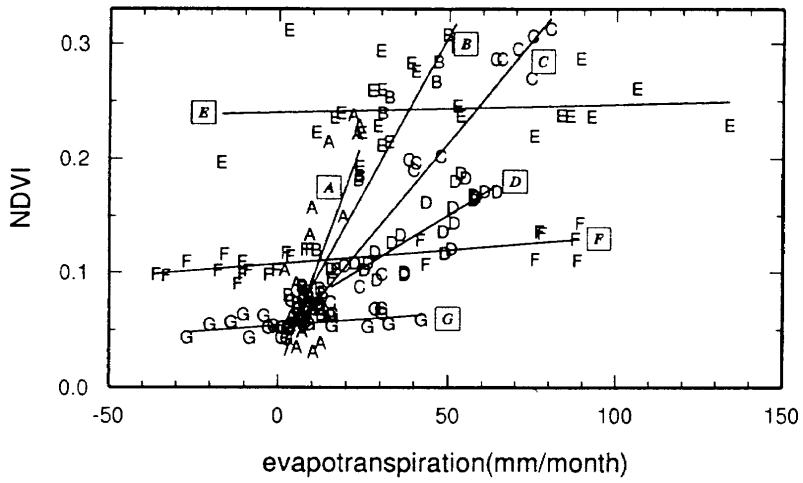

Fig. 6. The NDVI and ET relationships which are categorized into seven vegetation cover types.

ships were found. Over western and eastern Siberia, the annual marches of the ET and the NDVI were quite similar, and the correlation coefficient was very high. This suggests that the vegetational activity was closely related to the ET seasonal variation.

Bimodal annual variations were observed both in NDVI and ET seasonal change in Punjab, where bi-seasonal cultivation was seen. From this fact, the bimodal annual march of the ET may indicate the signal of bi-seasonal cultivation. The analyses for vegetation cover types and the ET–NDVI clarified that their relationships are distinguished among the vegetation types. The results presented in this paper may demonstrate the possibility of investigating the continental-scale vegetation activity and the ET, which is derived from assimilated gridded data.

Acknowledgments

We are grateful to Dr. T. Oki, Institute of Industrial Science, University of Tokyo, who provided us a computer program for the vapor flux computation. Moreover, we express our gratitude to Dr. Y. Honda,

Center for Environmental Remote Sensing, Chiba University, who provided us monthly GVI data. All pictures were constructed with the help of the GMT System (Wessel and Smith, 1991). This study was executed as a part of GEWEX Asian Monsoon Experiment (GAME) research activities, and partly supported by the Special Research Project on Global Environmental Change at the University of Tsukuba.

Appendix

Re-categorization of the original 59 vegetation types into seven types is shown. Descriptions of the original classification were simplified.

- CATEGORY A (Tundra/Polar Desert): Tundra; Wooded tundra margin or mountain; Polar desert with rock lichens
- CATEGORY B (Boreal Forest/Taiga): Main boreal conifer forest; Snowy non-boreal conifer forest; Cold steppe/meadow, Larch wood; Larch taiga with deciduous conifer; Northern or maritime taiga
- CATEGORY C (Cool Field/Cropland): Conifer/deciduous with snow in winter; Snowy deciduous forest; Cool farmland and settlements; Cool cropland with irrigation; Cold cropland and pasture; Cool grass/shrub; Mires including peaty bogs and fens; Cool/cold shrub semi-desert/steppe; Snowy field/woods complex; Snowy forest/field; Southern dry taiga or similar aspen/birch with northern and/or mountain conifers
- CATEGORY D (Warm Forest/Cropland): Temperate broadleaf/conifer forest; Mild/hot farm land and settlements; Paddy rice; Mild/warm/hot grass/shrub; Forest/field complex with regrowth after disturbances *etc.*; Field/woods with grass and/or cropland
- CATEGORY E (Tropical Forest): Tropical montane complexes; Tropical broadleaf seasonal; Rain-green (drought-deciduous) or very seasonal dry evergreen forests to open woodlands; Tropical rain forest
- CATEGORY F (Semi-Arid): Warm/hot cropland with irrigation; Succulent and thorn woods or scrub
- CATEGORY G (Desert): Stone, clay, or sand desert; Sand desert with dunes; Semi-desert/desert scrub/succulent/sparse grass; Salt/soda flats desert playas

References

Blondin, C., 1991: Parameterization of land-surface processes in numerical weather prediction. *"Land surface evaporation: measurement and parameterization"* (eds. T.J. Schmugge and J.-C. André), Springer-Verlag New York Inc., 31–54.

Brutsaert, W. and H. Stricker, 1979: An advection-aridity approach to estimate actual regional evapotranspiration. *Water Resour. Res.*, **15**, 443–450.

DeFries, R.S. and J.R.G. Townshend, 1994: NDVI-derived land cover classifications at a global scale. *Int. J. Remote Sensing*, **15**, 3567–3586.

EPA Global Climate Research Program and NOAA/NGDC Global Change Database Program, 1992: Global Ecosystems Database version 1.0. Global Change Database, Volume 1.

Honda, Y., S. Murai and K. Katoou, 1992: Global monitoring of vegetation. *J. of the Japan Soc. of Photogram. and Remote Sens.*, **31**, 4–14 (in Japanese).

Kalnay, E., M. Kanamitsu, R. Kistler, W. Collins, D. Deaven, L. Gandin, M. Iredell, S. Saha, G. White, J. Woollen, Y. Zhu, M. Chelliah, W. Ebisuzaki, W. Higgins, J. Janowiak, K.C. Mo, C. Ropelewski, J. Wang, A. Leetmaa, R. Reynolds, R. Jenne and D. Joseph, 1996: The NCEP/NCAR 40-year reanalysis project. *Bull. Amer. Meteor. Soc.*, **77**, 434–471.

Kondoh, A., 1995: Relationship between the global vegetation index and the evapotranspirations derived from climatological estimation methods. *J. of the Japan Soc. of Photogram. and Remote Sens.*, **34**, 6–14.

Malingreau, J.-P., 1986: Global vegetation dynamics: satellite observations over Asia. *Int. J. Remote Sensing*, **7**, 1121–1146.

Matsuyama, H., T. Oki, M. Shinoda and K. Masuda, 1994: The seasonal change of the water budget in the Congo river basin. *J. Meteor. Soc. Japan*, **72**, 281–299.

Morton, F.I., 1978: Estimating evapotranspiration from potential evaporation: practicality of an iconoclastic approach. *J. Hydrol.*, **38**, 1–32.

Murai, S. and Y. Honda, 1991: Global change monitoring using the NOAA global vegetation index and geo-information. *Asian-Pacific Remote Sensing Journal*, **4**, 63–73.

Norwine, J. and D.H. Greegor, 1983: Vegetation classification based on Advanced Very High Resolution Radiometer (AVHRR) satellite imagery. *Remote Sens. Environ.*, **13**, 69–87.

Oki, T., K. Musiake, H. Matsuyama and K. Masuda, 1995: Global atmospheric water balance and runoff from large river basins. *Hydrological Processes*, **9**, 655–678.

Peixoto, J.P. and A.H. Oort, 1983: The atmospheric branch of the hydrological cycle and climate. *"Variations in the global water budget"* (eds. A. Street-Perrott, M. Beran and R. Ratchiffe), Reidel, Norwell, MA, 5–65.

Peixoto, J.P. and A.H. Oort, 1992: *"Physics of climate."* American Institute of Physics, NY, 520pp.

Ripley, E.A. and R.E. Redmann, 1976: Grassland. *"Vegetation and the atmosphere Volume 2 Case study"* (ed. J.L. Monteith), Academic Press, London, 439pp.

Running, S.W. and R.R. Nemani, 1988: Relating seasonal patterns of the AVHRR vegetation index to simulated photosynthesis and transpiration of forests in different climates. *Int. J. Remote Sensing*, **24**, 347–367.

Running, S.W., R.R. Nemani, D.L. Peterson, L.E. Band, D.F. Potts and L.L. Pierce, 1989: Mapping regional forest evapotranspiration and photosynthesis by coupling satellite data with ecosystem simulation. *Ecology*, **70**, 1090–1101.

Sellers, P.J., B.W. Meeson, J.J. Closs, J. Collatz, F. Corprew, D. Dazlich, F.G. Hall, Y. Kerr, R. Koster, S. Los, K. Mitchell, J. McManus, D. Myers, K.-J. Sun and P. Try, 1996: The ISLSCP initiative I global datasets: surface boundary conditions and atmospheric forcings for land-atmosphere studies. *Bull. Amer. Meteor. Soc.*, **77**, 1987–2005.

Tarpley, J.D., S.R. Schneider and R.L. Money, 1984: Global vegetation indices from the NOAA-7 meteorological satellite. *J. Climate Appl. Meteor.*, **23**, 491–494.

Tarpley, J.D., 1991: The NOAA global vegetation index product—A review. *Palaeogeogr., Palaeoclimatol., Palaeoecol. (Global Planet. Change Sect.)*, **90**, 189–194.

Trenberth, K.E., 1991: Climate diagnostics from global analyses: Conservation of mass in ECMWF analyses. *J. Climate*, **4**, 707–722.

Trenberth, K.E. and J.G. Olson, 1988: An evaluation and intercomparison of global analyses from the National Meteorological Center and the European Centre for Medium Range Weather Forecasts. *Bull. Amer. Meteor. Soc.*, **69**, 1047–1057.

Trenberth, K.E. and C.J. Guillemot, 1995: Evaluation of the global atmospheric moisture budget as seen from analyses. *J. Climate*, **8**, 2255–2272.

Wessel, P. and W.H.F. Smith, 1991: Free software helps map and display data. *EOS Trans. AGU*, **72**, 441, 445–446.

Xie, P. and P.A. Arkin, 1995: An intercomparison of gauge observations and satellite estimates of monthly precipitation. *J. Appl. Meteor.*, **34**, 1143–1160.

Xie, P. and P.A. Arkin, 1996: Analyses of global monthly precipitation using gauge observations, satellite estimates and numerical model predictions. *J. Climate*, **9**, 840–858.

格子点気象データより推定されたアジア地域における蒸発散量と衛星観測による植生指数

鈴木力英
（地球フロンティア研究システム）
谷田貝亜紀代
（宇宙開発事業団地球観測データ解析研究センター）
安成哲三
（筑波大学地球科学系）

全球格子点月別降水量データと、ヨーロッパ中期予報センター (ECMWF) の 4 次元同化データより大気水収支法を使って月別の蒸発散量をアジア地域で推定した。この値と気象衛星 NOAA の観測による全球植生指数との季節変化を比べた。対象期間は 1987 年と 1988 年で、蒸発散量 (ET)、植生指数 (NDVI) 共に月別値で解析を行なった。その結果、両者の季節変化間には強い関係が発見された。東西シベリアにおいて推定された ET は冬季小さな値を示しているのに対し、5 月から突然増加を開始し、7 月に最大となる。NDVI は ET とほぼ同様の季節変化を示すことから、この ET の増加は夏季における植生の蒸散活動の活発化に一つの原因を求めることができよう。また、インドとパキスタンにまたがるパンジャブ地方で NDVI に 1 年に 2 回のピークを見る。これは、この地方で二毛作が行なわれているためであるが、推定された ET にも年に 2 回のピークが認められ、二毛作の影響が現れていることをうかがわせる。本研究で得られた結果は、大陸スケールでの植生と、全球格子点気象データより推定された蒸発散量との関係を解析することの有効性を示すだろう。